Inorganic Chemistry

Article

pubs.acs.org/IC

Formation Principles for Vanadium Selenites: The Role of pH on Product Composition

Jacob H. Olshansky,[†] Karina J. Wiener,[†] Matthew D. Smith,[†] Anahita Nourmahnad,[†] Max J. Charles,[†] Matthias Zeller,[‡] Joshua Schrier,[†] and Alexander J. Norquist*[,†]

[†]Department of Chemistry, Haverford College, Haverford, Pennsylvania 19041, United States

[‡]Department of Chemistry, Youngstown State University, Youngstown, Ohio 44555, United States

Supporting Information

ABSTRACT: A series of organically templated vanadium selenites has been prepared under mild hydrothermal conditions. Single crystals of $[C_5H_{14}N_2][(VO)_3(SeO_3)_2(HSeO_3)_4]$, $[C_5H_{14}N_2][VO(SeO_3)_2]$, $[(R)\text{-}C_5H_{14}N_2][(VO)_3(SeO_3)_2(HSeO_3)_4]$, and $[(S)\text{-}C_5H_{14}N_2][(VO)_3(SeO_3)_2(HSeO_3)_4]$ were grown from $VOSO_4$, SeO_2, and 2-methylpiperazine. Controlling the initial pH of the reaction mixture allows for one to select between the compounds found in the $VOSO_4/SeO_2$/2-methylpiperazine system, as the solution pH directly affects the relative ratio of the $HSeO_3^-$ and SeO_3^{2-} concentrations. Moreover, partial resolution of racemic 2-methylpiperazine is observed in $[C_5H_{14}N_2][(VO)_3(SeO_3)_2(HSeO_3)_4]$, which is understood through the use of a one-dimensional Ising model. The use of enantiomerically pure 2-methylpiperazine results in fully ordered and fully resolved structures.

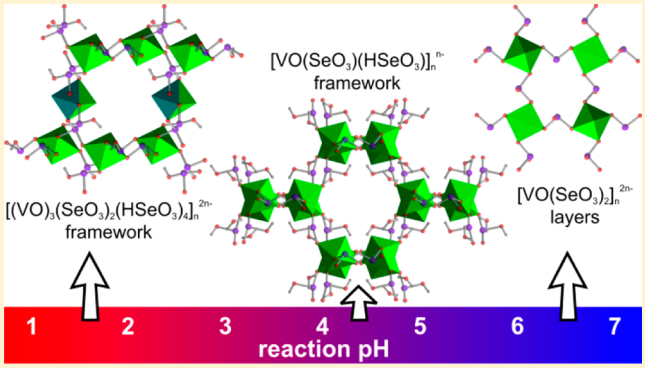

INTRODUCTION

A host of new materials has been prepared using hydrothermal and solvothermal reaction conditions during the past few decades.[1−5] These reaction conditions are especially attractive for exploratory work because they promote the growth of large single crystals, can be tuned to accommodate nearly any metal on the periodic table, and offer an astounding amount of phase space to search.[6] Metal oxides have been the focus of much of this work, owing to their structural diversity,[7,8] and ability to exhibit technologically advantageous properties.[9]

While the formation of new metal oxo compounds has been the focus of intense research for many years, the *a priori* design of novel materials with specific structures remains elusive, since the mechanisms by which they form are largely unknown.[10] Postulated mechanisms[4,7,11−13] have led to the elucidation of the reaction influences that most strongly affect the nature of the resulting products. These include (in order of strength) reactant concentrations,[14−22] charge density matching,[4,7,23−30] and a series of weaker influences, such as hydrogen-bonding,[30−32] sterics,[9,29] and symmetry.[33,34] In order to fully understand these influences, a wide range of reaction conditions must be explored through variation of reaction parameters such as temperature, time, pH, and reactant choice, all of which are known to affect the primary building units from which the products are formed.[6]

This study is designed to directly probe the effects of reaction mixture pH and reactant concentrations on the compositions of the resulting products. A series of organically templated vanadium selenites containing the $[2\text{-methylpiperazineH}_2]^{2+}$ cations is reported. $[C_5H_{14}N_2][(VO)_3(SeO_3)_2(HSeO_3)_4]$ (**1a**/**1b**) and $[C_5H_{14}N_2][VO(SeO_3)_2]$ (**2**) were synthesized from racemic sources of 2-methylpiperazine, while $[(R)\text{-}C_5H_{14}N_2][(VO)_3(SeO_3)_2(HSeO_3)_4]$ (**3a**) and $[(S)\text{-}C_5H_{14}N_2][(VO)_3(SeO_3)_2(HSeO_3)_4]$ (**3b**) were grown from enantiomerically pure (*R*)-(−)-2-methylpiperazine and (*S*)-(+)-2-methylpiperazine, respectively.

EXPERIMENTAL SECTION

Materials. $VOSO_4$ (97%) was purchased from Aldrich. SeO_2 (99.4%), 2-methylpiperazine (2-mpip, 95%), (*R*)-(−)-2-methylpiperazine ((*R*)-2-mpip, 98+%), and (*S*)-(+)-2-methylpiperazine ((*S*)-2-mpip, 98+%) were purchased from Alfa Aesar. All reagents were used as received. Deionized water was used in these syntheses.

Synthesis. All reactions were conducted in 23 mL poly(fluoroethylene-propylene) lined pressure vessels. Initial reaction pHs were controlled by the addition of 4 M HCl and 4 M NaOH. Reactions were heated to 110 °C and allowed to soak for 24 h. The reactions were then cooled to room temperature at a rate of 6 °C·h^{-1} to promote the growth of large single crystals. Autoclaves were opened in air, and products were recovered through filtration. No additional crystalline or amorphous reaction products were observed.

$[C_5H_{14}N_2][(VO)_3(SeO_3)_2(HSeO_3)_4]$ (1). **1** was synthesized as single crystals through the reaction of 0.1644 g (1.009×10^{-3} mol) of $VOSO_4$, 0.6662 g (6.004×10^{-3} mol) of SeO_2, 0.3025 g (3.517×10^{-3}

Received: July 18, 2014
Published: November 3, 2014

   dx.doi.org/10.1021/ic501736r | Inorg. Chem. 2014, 53, 12027−12035

Table 1. Crystallographic Data for Compounds 1a−3b

	$[C_5H_{14}N_2][(VO)_3(SeO_3)_2(HSeO_3)_4]$ (1a)	$[C_5H_{14}N_2][(VO)_3(SeO_3)_2(HSeO_3)_4]$ (1b)	$[C_5H_{14}N_2][VO(SeO_3)_2]$ (2)	$[(R)\text{-}C_5H_{14}N_2][(VO)_3(SeO_3)_2(HSeO_3)_4]$ (3a)	$[(S)\text{-}C_5H_{14}N_2][(VO)_3(SeO_3)_2(HSeO_3)_4]$ (3b)
formula	$C_5H_{18}N_2O_{21}Se_6V_3$	$C_5H_{18}N_2O_{21}Se_6V_3$	$C_5H_{18}N_2O_7Se_2V_1$	$C_5H_{18}N_2O_{21}Se_6V_3$	$C_5H_{18}N_2O_{21}Se_6V_3$
fw	1068.79	1068.79	423.04	1068.79	1068.79
space group	$P1$ (No. 1)	$P1$ (No. 1)	$P2_1$ (No. 4)	$P1$ (No. 1)	$P1$ (No. 1)
a/Å	8.031(3)	8.0532(17)	7.9731(15)	8.0024(14)	8.0016(12)
b/Å	8.923(3)	8.9284(19)	8.6063(16)	8.8989(16)	8.9089(14)
c/Å	9.111(3)	9.111(2)	8.7810(16)	9.1287(16)	9.1270(14)
α/deg	93.598(4)	93.563(3)	90	93.868(2)	93.9196(18)
β/deg	108.804(4)	108.910(2)	90.023(2)	108.723(2)	108.7243(16)
γ/deg	103.521(4)	103.594(3)	90	103.234(2)	103.2235(17)
V/Å^3	594.1(3)	595.5(2)	602.54(19)	592.28(18)	592.71(16)
Z	1	1	2	1	1
ρ_{calc}/g cm^{-3}	2.987	2.980	2.332	2.996	2.994
λ/Å	0.71073	0.71073	0.71073	0.71073	0.71073
T/K	100(2)	100(2)	100(2)	100(2)	100(2)
μ/mm^{-1}	10.444	10.419	6.888	10.477	10.469
Flack param	0.050(19)	0.181(16)	0.455(17)	0.027(8)	0.034(8)
R1[a]	0.0367	0.0237	0.0319	0.0206	0.0227
wR2[b]	0.0922	0.0586	0.0814	0.0500	0.0577

[a] $R1 = \sum||F_o| - |F_c||/\sum|F_o|$. [b] $wR2 = [\sum w(F_o^2 - F_c^2)^2/[\sum w(F_o^2)^2]]^{1/2}$.

mol) of 2-mpip, and 5.9980 g (3.33×10^{-1} mol) of H_2O. Blue blocks were produced in 79.6% yield (based upon V). IR data (cm^{-1}): N−H, 1441, 1466, 1572; C−H, 3027; O−H, 3431; V═O, 965; Se−O, 814. EA obsd (calc): C 5.82% (5.61%), H 1.47% (1.70%), N 2.57% (2.60%), Se 37.7% (44.3%), V 13.3% (14.3%).

$[C_5H_{14}N_2][VO(SeO_3)_2]$ (2). **2** was synthesized as single crystals through the reaction of 0.3234 g (1.984×10^{-3} mol) of $VOSO_4$, 0.5607 g (5.053×10^{-3} mol) of SeO_2, 0.4065 g (4.727×10^{-3} mol) of 2-mpip, and 3.378 g (1.88×10^{-1} mol) of H_2O. Aquamarine plates were produced in 27.8% yield (based upon V). IR data (cm^{-1}): N−H, 1452, 1618; C−H, 3007; O−H, 3449; V═O, 982; Se−O, 810. EA obsd (calc): C 14.33% (14.19%), H 1.75% (3.3%), N 2.5% (6.6%), Se 41.66% (37.3%), V 13.77% (12.0%).

$[(R)\text{-}C_5H_{14}N_2][(VO)_3(SeO_3)_2(HSeO_3)_4]$ (3a). **3a** was synthesized as single crystals through the reaction of 0.1624 g (9.96×10^{-4} mol) of $VOSO_4$, 1.5624 g (1.408×10^{-2} mol) of SeO_2, 0.0537 g (6.24×10^{-4} mol) of (*R*)-2-mpip, and 5.292 g (2.94×10^{-1} mol) of H_2O. Blue blocks were produced in 73.2% yield (based upon V). IR data (cm^{-1}): N−H, 1440, 1466, 1575; C−H, 3029; O−H, 3421; V═O, 966; Se−O, 854. EA obsd (calc): C 5.61% (5.61%), H 1.72% (1.70%), N 2.58% (2.60%), Se 43.73% (44.3%), V 13.92% (14.3%).

$[(S)\text{-}C_5H_{14}N_2][(VO)_3(SeO_3)_2(HSeO_3)_4]$ (3b). **3b** was synthesized as single crystals through the reaction of 0.1655 g (1.015×10^{-3} mol) of $VOSO_4$, 1.5661 g (1.411×10^{-2} mol) of SeO_2, 0.104 g (1.209×10^{-3} mol) of (*S*)-2-mpip, and 5.9500 g (3.310×10^{-1} mol) of H_2O. Blue blocks were produced in 84.2% yield (based upon V). IR data (cm^{-1}): N−H, 1440, 1466, 1573; C−H, 3027; O−H, 3420; V═O, 966; Se−O, 854. EA obsd (calc): C 5.41% (5.61%), H 1.68% (1.70%), N 2.89% (2.60%), Se 41.88% (44.3%), V 13.53% (14.3%).

Single Crystal X-ray Diffraction. Data were collected using a Bruker AXS Smart Apex CCD diffractometer with Mo Kα radiation (λ = 0.71073 Å). A single crystal was mounted on a Mitegen micromesh mount using a trace of mineral oil and cooled *in situ* to 100(2) K for data collection. Frames were collected, reflections were indexed and processed, and the files were scaled and corrected for absorption using APEX2.[35] The heavy atom positions were determined using SIR92.[36] All other non-hydrogen sites were located from Fourier difference maps. All non-hydrogen sites were refined using anisotropic thermal parameters using full matrix least-squares procedures on F_o^2 with $I > 3\sigma(I)$. Hydrogen atoms were placed in geometrically idealized positions. All calculations were performed using Crystals v. 14.23c.[37] Relevant crystallographic data are listed in Table 1. A figure displaying the positions of the largest peak and hole in the difference map for compound **2** can be found in the Supporting Information.

Powder X-ray Diffraction. Powder diffraction patterns were recorded on a GBC-Difftech MMA powder diffractometer. Dry powdered samples were packed into sample holders. Calculated powder patterns were generated from single crystal data using ATOMS v. 6.0.[38] Powder X-ray diffraction patterns were consistent with patterns predicted from the refined structures of **1**−**3**. No evidence of additional phases was observed. Experimental powder X-ray diffraction patterns match patterns simulated from single crystal diffraction data.

Infrared Spectroscopy. Infrared measurements were obtained using a PerkinElmer FT-IR Spectrum 1000 spectrophotometer. Samples were diluted with spectroscopic grade KBr and pressed into pellets. Scans were collected over the range of 400−4000 cm^{-1}.

Bond Valence Sums. The hydrogen-bonding networks present in all compounds were analyzed using bond valence sums.[39] All calculations were performed using parameters compiled by Brese and O'Keeffe.[40] Complete tables of bond valence sums for each compound are available in the Supporting Information.

Electronic Structure Calculations. Solid-state electronic structure calculations were performed using ABINIT v. 6.4.1.[41,42] ABINIT calculations used the Perdew−Burke−Ernzerhof generalized gradient approximation (PBE-GGA) exchange-correlation functional, norm-conserving Troullier−Martins pseudopotentials, a planewave basis set with energy cutoff of 25 hartree, a 6 × 6 × 6 Monkhorst−Pack *k*-point sampling grid, and experimental crystal structures. Electron localization functions (ELFs) were calculated from the self-consistent valence electron densities and visualized using Vesta v. 3.1.8.[43] Partial atomic charge determinations were performed using the iterative-Hirshfeld scheme (Hirshfeld-I)[44,45] on the self-consistent valence electron density using the Cut3D program and promolecular all-electron atomic charge densities were using the HF96 atomic Hartree−Fock code[46] following the method described in our previous work.[9,29,31,47,48]

dx.doi.org/10.1021/ic501736r | Inorg. Chem. 2014, 53, 12027−12035

RESULTS AND DISCUSSION

The inorganic components in compounds **1**−**3b** are all constructed from similar primary building units. Compounds **1**, **3a**, and **3b** contain $[VO_5]$, $[VO_6]$, $[HSeO_3]^-$, and $[SeO_3]^{2-}$ moieties, while **2** only contains $[VO_5]$ and $[SeO_3]^{2-}$ groups. The $V-O_{terminal}$ bond lengths range between 1.582(8) and 1.6189(4) Å, while the $V-O_{bridging}$ bonds are longer, between 1.863(8) and 2.215(3) Å. $Se-O_{bridging}$ bond lengths are observed between 1.660(3) and 1.731(5) Å. Se−O(H) bonds are longer, with distances between 1.754(6) and 1.7918(4) Å. The bond valence sums for vanadium and selenium range between 3.93 and 4.10 vu and between 3.87 and 4.17 vu, respectively. Complete tables of bond lengths and angles can be found in .cif format in the Supporting Information.

$[C_5H_{14}N_2][(VO)_3(SeO_3)_2(HSeO_3)_4]$ (**1**) contains a three-dimensional inorganic framework and $[2\text{-mpipH}_2]^{2+}$ cations. The $[2\text{-mpipH}_2]^{2+}$ cations reside in channels within the framework, as shown in Figure 1. The framework is constructed

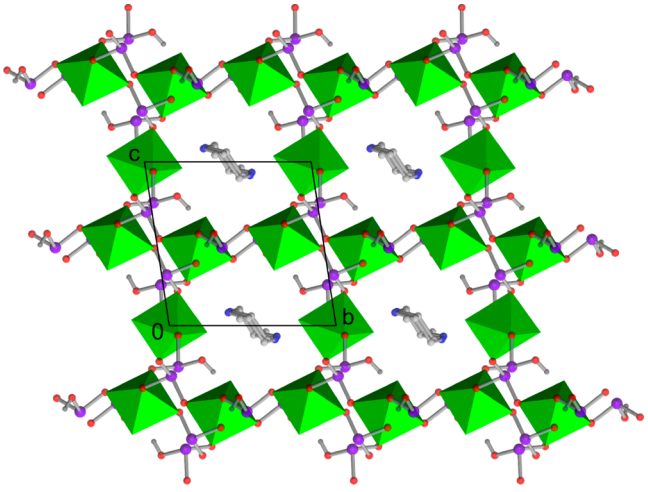

Figure 1. Three-dimensional packing of $[C_5H_{14}N_2][(VO)_3(SeO_3)_2(HSeO_3)_4]$ (**1**). Green polyhedra represent $[VO_6]$ and $[VO_5]$, while purple, red, blue, white, and gray spheres represent selenium, oxygen, nitrogen, carbon, and hydrogen, respectively. Organic ammonium cation hydrogen atoms have been omitted for clarity.

from two distinct components. $[(VO)(SeO_3)(HSeO_3)]$ chains, which extend along the [1 1 0] direction, form hydrogen-bonded pseudolayers. Similar chain connectivities have been observed in a series of metal selenites.[49,50] $[(VO)(HSeO_3)_2]$ groups act as pillars between the pseudolayers, forming the three-dimensional framework. Compound **1** was synthesized from a racemic mixture of 2-mpip. Partial resolution of the $[(R)\text{-2-mpipH}_2]^{2+}$ and $[(S)\text{-2-mpipH}_2]^{2+}$ cations is observed, which is discussed below. Crystallographic disorder is observed in both the organic ammonium cations and $[VO_5]$ square pyramids.

$[C_5H_{14}N_2][VO(SeO_3)_2]$ (**2**) contains $[VO(SeO_3)_2]_n^{2n-}$ layers separated by $[2\text{-mpipH}_2]^{2+}$ cations. See Figure 2. The $[VO(SeO_3)_2]_n^{2n-}$ layers in **2** are similar to those observed in $(H_3NCH_2CH_2NH_3)[VO(SeO_3)_2]$, a related phase containing ethylenediammonium cations.[51] Additional analogues are found in both organically templated compounds[52] and inorganic phases.[53−55] Compound **2** exists as an inversion twin, in which the $[(R)\text{-2-mpipH}_2]^{2+}$ and $[(S)\text{-2-mpipH}_2]^{2+}$ cations are segregated into domains within each crystal. The Hirshfeld-I

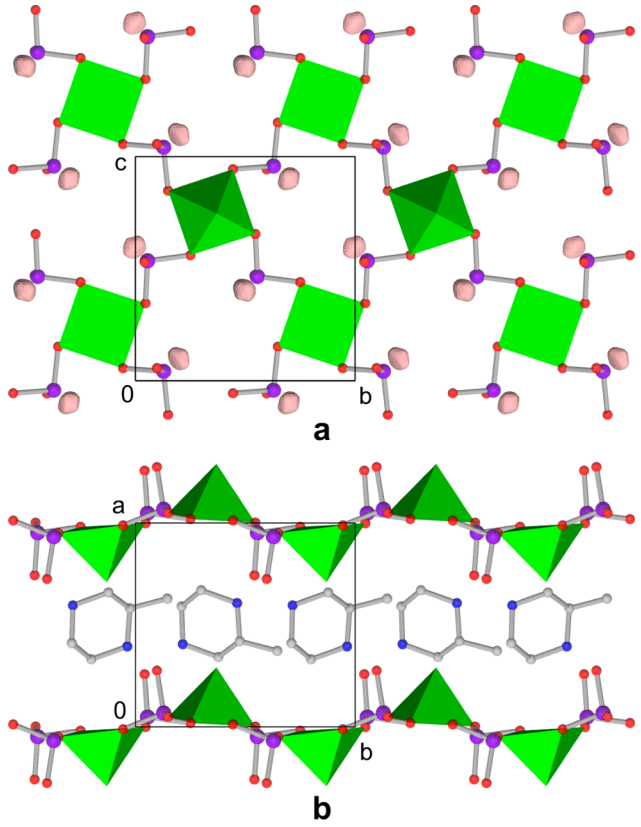

Figure 2. Views of the (a) $[VO(SeO_3)_2]_n^{2n-}$ layers and (b) three-dimensional packing for $[C_5H_{14}N_2][VO(SeO_3)_2]$ (**2**). ELF isosurfaces are shown with a boundary condition of 0.96. Green polyhedra represent $[VO_5]$, while purple, red, blue, and white spheres represent selenium, oxygen, nitrogen, and carbon, respectively. Hydrogen atoms have been omitted for clarity.

scheme[44,45,56] was used to determine partial atomic charges for all atoms; a complete table of partial atomic charges for **2** is available in the Supporting Information. As **2** crystallizes in the chiral and polar space group *P*1 (No. 1), the magnitudes and directions of both component and net dipole moments were calculated.[9,29,30,47,57−59] See Figure 3 and Table 2. Pseudoinversion within the inorganic component is observed, with a near cancellation in the dipole moment of the $[VO(SeO_3)_2]_n^{2n-}$ layers. The $[(R)\text{-2-mpipH}_2]^{2+}$ cations, in contrast, are roughly aligned with the *b*-axis and make the largest contribution to the net dipole moment.

Compounds **1** and **2** were synthesized from the $VOSO_4/SeO_2$/2-mpip system. We recently published another compound from this system, $[C_5H_{14}N_2][VO(SeO_3)(HSeO_3)]_2 \cdot 2H_2O$,[30] which is constructed from the same primary building units as **1** and **2**, and exhibits a three-dimensional inorganic framework that is distinctly different from that in **1**. The major differences between these compounds stem from the ratios of components, as summarized in Table 3. As three compounds with different stoichiometries and structures were synthesized from the same reactants under nearly identical conditions, the influences that direct formation of each compound were investigated and elucidated.

During the past several years, we have observed a hierarchy of influences that affect the formation of organically templated metal oxides. The *primary influence* in these reactions is the relative concentration of each reactive species. The identities of these primary building units are dictated by experimental

dx.doi.org/10.1021/ic501736r | Inorg. Chem. 2014, 53, 12027−12035

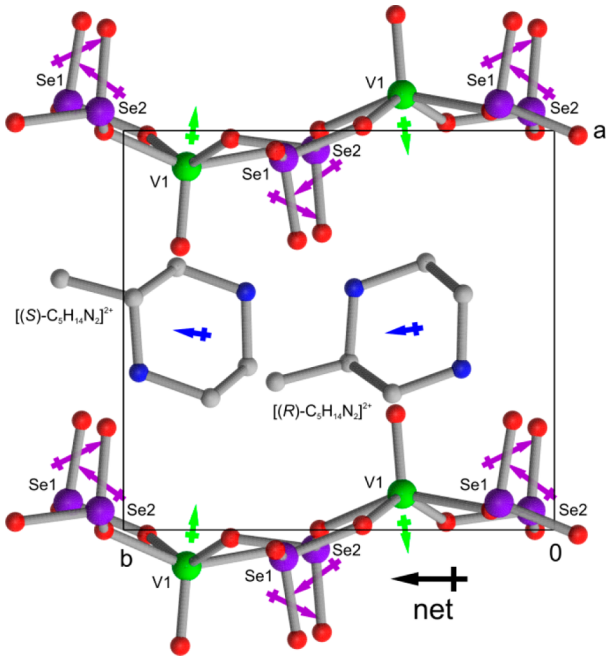

Figure 3. Ball-and-stick representation of **2**. Arrows indicate the approximate directions and magnitudes of the dipole moments for $[VO_5]$, $[SeO_3]$, and $[C_5H_{14}N_2]^{2+}$ cations. The large black arrow represents the direction of the net dipole moment for **2**. Hydrogen atoms have been omitted for clarity.

Table 2. Calculated Component and Net Dipole Moments for $[C_5H_{14}N_2][VO(SeO_3)_2]$ (2)

species	dipole moment (D)
$V(1)O_5$	3.87
$Se(1)O_3$	9.12
$Se(2)O_3$	9.04
$[VO(SeO_3)_2]^{2-}$ layer	0.53
$[2\text{-mpipH}_2]^{2+}$ cation	2.69
net	2.42

Table 3. Composition Ratios in $[C_5H_{14}N_2][VO(SeO_3)(HSeO_3)]_2{\cdot}2H_2O$, $[C_5H_{14}N_2][(VO)_3(SeO_3)_2(HSeO_3)_4]$ (1), and $[C_5H_{14}N_2][VO(SeO_3)_2]$ (2)

compound	V:Se:amine ratio	$[HSeO_3]^-$:$[SeO3]^{2-}$ ratio
$[C_5H_{14}N_2][(VO)_3(SeO_3)_2(HSeO_3)_4]$ (**1**)	3:6: 1	2:1
$[C_5H_{14}N_2][VO(SeO_3)(HSeO_3)]_2{\cdot}2H_2O$	2:4:1	1:1
$[C_5H_{14}N_2][VO(SeO_3)_2]$ (**2**)	1:2:1	0:2

parameters, such as pH, temperature, and even reactant choice. The relative concentrations of the reactive species also directly influence composition and structure.[14−21,29,31] The *secondary influence* is charge density matching[4,7] between the inorganic anionic and organic cationic components of these reactions. While the charge densities of the organic cations are largely fixed by solution pH, as that dictates their protonation states, the inorganic components can access a range of charge densities through the formation of different secondary building units (SBUs).[27,28,31] Several weaker *tertiary influences* have also been observed, which neither dictate the compositions of the compounds nor control the connectivities of their respective SBUs. Instead, they generally affect local bonding interactions and involve subtle structural parameters, such as hydrogen bonding,[31,32,48] sterics,[33] or symmetry.[12,14−16,22,33,34] The effects of reactant concentrations as a primary influence are clearly observed in the work reported here, through their manipulation using both initial pH and reaction mixture compositions. In addition, tertiary infleunces are observed in the partial resolution of racemic 2-mpip in **1**.

The effects of reactant concentrations in the $VOSO_4/SeO_2$/2-mpip system were explored in two ways. First, three series of reactions were conducted, each of which contained a specific fixed V:Se:amine ratio. Second, the initial solution pH was varied between 1 and 7 for each V:Se:amine ratio. Distinct crystallization fields for **1**, **2**, and $[C_5H_{14}N_2][VO(SeO_3)(HSeO_3)]_2{\cdot}2H_2O$ are observed throughout this range of reaction conditions, as shown in Figure 4.

The initial solution pH of each reaction mixture affects the relative phase stabilities of **1**, **2**, and $[C_5H_{14}N_2][VO(SeO_3)(HSeO_3)]_2{\cdot}2H_2O$. The $[HSeO_3]^-$:$[SeO_3]^{2-}$ ratio varies in the three compounds observed in the $VOSO_4/SeO_2$/2-mpip system. See Table 3. **1** is the most $[HSeO_3]^-$ rich compound in the system with a $[HSeO_3]^-$:$[SeO_3]^{2-}$ ratio of 2:1. $[C_5H_{14}N_2][VO(SeO_3)(HSeO_3)]_2{\cdot}2H_2O$, in contrast, contains an equal number of $[HSeO_3]^-$ and $[SeO_3]^{2-}$ groups. **2** only contains $[SeO_3]^{2-}$ and is the most $[SeO_3]^{2-}$ rich compound. **1** is observed at low pH conditions, under which $[HSeO_3]^-$ is stabilized with respect to $[SeO_3]^{2-}$. As the initial solution pH increases, so does the relative concentration of $[SeO_3]^{2-}$ with respect to $[HSeO_3]^-$. This causes a shift in phase stability to $[C_5H_{14}N_2][VO(SeO_3)(HSeO_3)]_2{\cdot}2H_2O$, which contains an equal amount of $[HSeO_3]^-$ and $[SeO_3]^{2-}$. **2**, which only contains $[SeO_3]^{2-}$, is only observed from reactions with the highest initial solution pHs. Clearly, the relative concentrations of $[HSeO_3]^-$ and $[SeO_3]^{2-}$ in solution are reflected in the compositions of the resulting compounds.

The relative phase stabilities of **1**, **2**, and $[C_5H_{14}N_2][VO(SeO_3)(HSeO_3)]_2{\cdot}2H_2O$ are also affected by the initial concentrations of vanadium, selenium, and 2-mpip. See Figure 4. The crystallization fields of these three compounds shift as the initial reaction mixture is changed from 1 V : 8 Se : 1 amine to 1 V : 6 Se : 3 amine, a change in which the initial amine concentration is drastically increased. **2** is the most amine rich compound, with a V:Se:amine ratio of 1:2:1, while $[C_5H_{14}N_2][VO(SeO_3)(HSeO_3)]_2{\cdot}2H_2O$ and **1** are both more vanadium deficient. As such, increasing the initial amine concentration stabilizes the formation of **2** with respect to $[C_5H_{14}N_2][VO(SeO_3)(HSeO_3)]_2{\cdot}2H_2O$ and **1**, and causes the crystallization field of **2** to increase. Likewise, $[C_5H_{14}N_2][VO(SeO_3)(HSeO_3)]_2{\cdot}2H_2O$ is stabilized with respect to **1**, owing to the low amine concentration in **1**. This causes an analogous shift in the crystallization field of $[C_5H_{14}N_2][VO(SeO_3)(HSeO_3)]_2{\cdot}2H_2O$ to lower pHs, and results in cocrystallization of **1** and $[C_5H_{14}N_2][VO(SeO_3)(HSeO_3)]_2{\cdot}2H_2O$ at pH 2 (shown as green in Figure 4).

The results of doubling the vanadium concentration are shown in the 2 V:5 Se:3 amine portion of Figure 4. The crystallization field corresponding to compound **2** is no longer observed because this compound, which has the lowest vanadium concentration, is destabilized by the vanadium rich reaction mixture. The crystallization fields of **1** and $[C_5H_{14}N_2][VO(SeO_3)(HSeO_3)]_2{\cdot}2H_2O$ do not change appreciably.

dx.doi.org/10.1021/ic501736r | *Inorg. Chem.* 2014, 53, 12027−12035

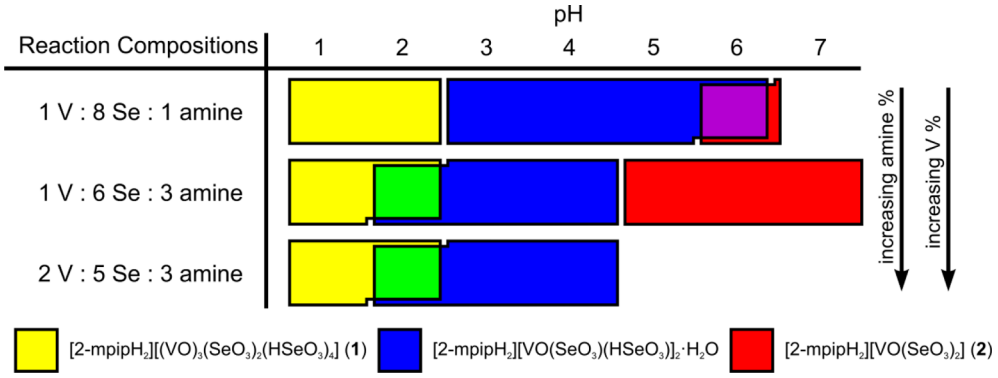

Figure 4. Plot of the product composition as a function of solution pH and initial reaction mixture composition in the $VOSO_4/SeO_2$/2-mpip/H_2O system.

The phase stabilities of **1**, **2**, and $[C_5H_{14}N_2][VO(SeO_3)(HSeO_3)]_2{\cdot}2H_2O$ are directly affected by the concentrations of the primary building units, from which they are formed. These effects were directly observed either by changing the initial vanadium, selenium, and amine concentration or by changing the protonation state of the selenous acid by altering the initial reaction pH. The relative concentrations of the primary building units are the strongest influence over the composition and structure of the resulting compounds.

1 was synthesized from a racemic mixture of (*R*)-2-mpip and (*S*)-2-mpip. Disorder is present in the crystallographic structure of **1**, in which an $[(R)\text{-2-mpipH}_2]^{2+}$ and an $[(S)\text{-2-mpipH}_2]^{2+}$ cation roughly occupy the same site of the structure. The central piperazinium rings in the $[(R)\text{-2-mpipH}_2]^{2+}$ and $[(S)\text{-2-mpipH}_2]^{2+}$ cations are not superimposed. Instead, each atom in each cation resides on its own site, as shown in Figure 5. Disorder is also present in the $[V(3)O_5]$ and $[V(4)O_5]$ polyhedra. The $[(R)\text{-2-mpipH}_2]^{2+}$ and $[(S)\text{-2-mpipH}_2]^{2+}$ cations in **1** are not related to one another through any symmetry operation, making this compound a group 2 kryptoracemate, as defined by Brock et al.[60] In addition, the populations of $[(R)\text{-2-mpipH}_2]^{2+}$ and $[(S)\text{-2-mpipH}_2]^{2+}$ within each crystal differ; they are not present in a 1:1 ratio, despite the crystals being grown from a solution containing a racemic mixture of 2-mpip. Single crystal X-ray diffraction data were collected on seven different crystals of **1**. The results of population refinements of the $[(R)\text{-2-mpipH}_2]^{2+}$ and $[(S)\text{-2-mpipH}_2]^{2+}$ cations in these seven crystals are summarized in Table 4. While there is no preference for either $[(R)\text{-2-mpipH}_2]^{2+}$ or $[(S)\text{-2-mpipH}_2]^{2+}$, the cations consistently appear in a ratio of ~2:1. The mean and median ratios are 68.2:31.8 and 67.7:32.3, respectively. The structures denoted **1a** and **1b** in Table 1 represent results from two different single crystals, one of which contains more $[(R)\text{-2-mpipH}_2]^{2+}$ (**1a**), while the other contains more $[(S)\text{-2-mpipH}_2]^{2+}$ (**1b**). The structures of the other five single crystals are essentially identical to either **1a** or **1b**, and so their inclusion would be redundant.

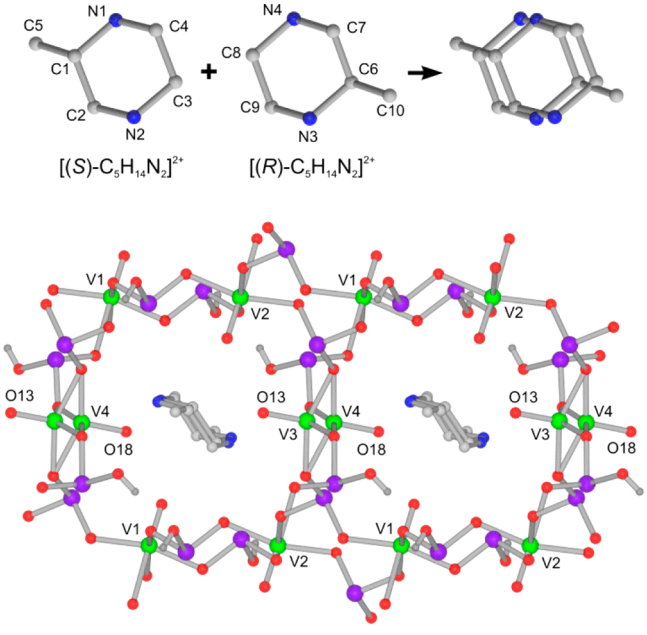

Figure 5. Disorder mechanism for the $[C_5H_{14}N_2]^{2+}$ cations and the $[VO_5]$ polyhedra in **1**. Hydrogen atoms on the organic cations have been omitted for clarity.

Table 4. Refined Occupancies of $[(R)\text{-2-mpipH}_2]^{2+}$ and $[(S)\text{-2-mpipH}_2]^{2+}$ in Compounds 1 and 3

compound	$[(R)\text{-2-mpipH}_2]^{2+}$ percentage	$[(S)\text{-2-mpipH}_2]^{2+}$ percentage
compound **1a**	30.8	69.2
compound **1b**	71.3	28.7
	67.7	32.3
	33.2	66.8
	68.3	31.7
	33.4	66.6
	67.4	32.6
compound **3a**	100	0
compound **3b**	0	100

The partial resolution of the (*R*)-2-mpip and (*S*)-2-mpip in the formation of **1** prompts two questions. First, what is the basis for the resolution of (*R*)-2-mpip and (*S*)-2-mpip in this reaction? Second, can enantiomerically pure analogues be formed and can their structures help explain the partial resolution in **1**? In order to address these questions, reactions using enantiomerically pure sources of either (*R*)-2-mpip or (*S*)-2-mpip were conducted. The results of these reactions are $[(R)\text{-}C_5H_{14}N_2][(VO)_3(SeO_3)_2(HSeO_3)_4]$ (**3a**) and $[(S)\text{-}C_5H_{14}N_2][(VO)_3(SeO_3)_2(HSeO_3)_4]$ (**3b**). See Figure 6.

3a and **3b** crystallize in *P*1 (No. 1), and the Flack parameters indicate well-resolved absolute structures, with values of 0.027(8) and 0.034(8) for **3a** and **3b**, respectively. There is

dx.doi.org/10.1021/ic501736r | *Inorg. Chem.* 2014, 53, 12027−12035

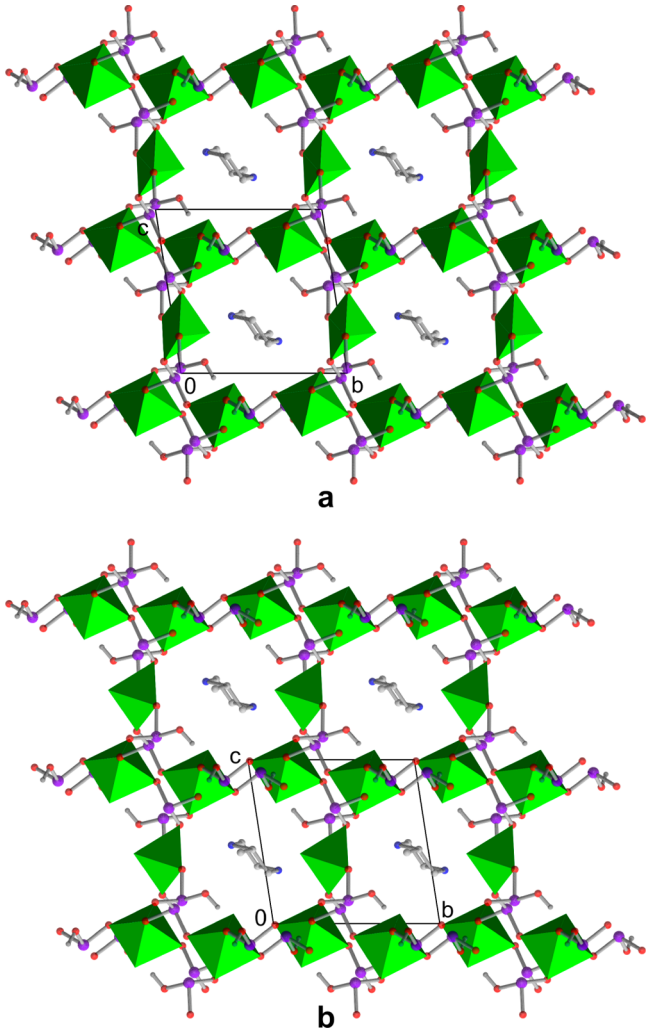

Figure 6. Three-dimensional packing figures for **3a** and **3b**. Green polyhedra represent $[VO_6]$ and $[VO_5]$, while purple, red, blue, white, and gray spheres represent selenium, oxygen, nitrogen, carbon, and hydrogen, respectively. Organic ammonium cation hydrogen atoms have been omitted for clarity.

no crystallographic disorder in either the inorganic or organic components of these compounds. The orientations of the $[VO_5]$ pillars are resolved, as shown in Figure 6. Dipole moment calculations were performed on **3a** and **3b**, with results summarized in Table 5. Pseudoinversion symmetry is observed in the component dipole moments of $[V(2)O_6]$, $[V(3)O_6]$, and all $[SeO_3]^{2-}$ and $[HSeO_3]^{-}$ groups, as shown in Figure 7. The component moment of $[V(1)O_5]$ makes the largest contribution to the net framework moments, which are calculated to be 4.03 and 2.99 D for **3a** and **3b**, respectively. The dipole moments on the $[2\text{-mpipH}_2]^{2+}$ cations are roughly anti-aligned with respect to the $[V(1)O_5]$ square pyramids, resulting in net compound moments of 2.70 and 2.23 D for **3a** and **3b**, respectively. Differences in dipole moments of this magnitude within pairs of enantiomer structures are common.[9,29,30,47] These differences are generally caused by asymmetric charge distributions on the $[(R)\text{-2-mpipH}_2]^{2+}$ and $[(S)\text{-2-mpipH}_2]^{2+}$ cations and the orientation of O−H bonds in the $[HSeO_3]^{-}$ groups.

The structures of **3a** and **3b** provide useful information to understand the partial resolution of the organic ammonium

Table 5. Calculated Component and Net Dipole Moments $[(R)\text{-}C_5H_{14}N_2][(VO)_3(SeO_3)_2(HSeO_3)_4]$ (3a) and $[(S)\text{-}C_5H_{14}N_2][(VO)_3(SeO_3)_2(HSeO_3)_4]$ (3b)

species	dipole moment (D)	
	compound **3a**	compound **3b**
$V(1)O_5$	3.67	3.61
$V(2)O_6$	8.79	8.75
$V(3)O_6$	8.42	8.42
$Se(1)O_3$	9.75	9.70
$Se(2)O_3$	9.87	9.82
$HSe(3)O_3$	11.16	11.04
$HSe(4)O_3$	11.16	11.18
$HSe(5)O_3$	10.97	10.84
$HSe(6)O_3$	10.87	10.99
$[(VO)_3(SeO_3)_2(HSeO_3)_4]^{2-}$ framework	4.03	2.99
$[2\text{-mpipH}_2]^{2+}$ cation	2.85	2.79
net	2.70	2.23

cations in **1**. The disorder of the $[2\text{-mpipH}_2]^{2+}$ cations and $[VO_5]$ polyhedra is not fully random. Instead, a partial ordering scheme is present in which the chirality of the $[2\text{-mpipH}_2]^{2+}$ cations and the orientations of the $[VO_5]$ polyhedra are conserved within the *ab* plane. An $[(R)\text{-2-mpipH}_2]^{2+}$ and an $[(S)\text{-2-mpipH}_2]^{2+}$ cation cannot sit next to one another within a given channel owing to steric repulsions between the methyl groups. Moreover, the position of the methyl group on a given $[2\text{-mpipH}_2]^{2+}$ cation directly affects the orientations of the adjacent $[VO_5]$ groups. This partial ordering scheme is also supported by the structures of **3a** and **3b**. The correlation between amine chirality and $[VO_5]$ polyhedron orientation in the partial ordering scheme is directly observed in these fully resolved structures. A figure of these interactions is provided in the Supporting Information. The disorder must come from weak correlations along the *c*-axis.

Differences in the three-dimensional hydrogen-bonding networks exist between fully resolved and mixed enantiomer compounds. The ring structures of the $[(R)\text{-2-mpipH}_2]^{2+}$ and $[(S)\text{-2-mpipH}_2]^{2+}$ cations in **1** are not superimposed. See Figure 5. As a result, the nature of the hydrogen-bonding interactions between the cation and inorganic framework depends upon the local chirality. N1 and N3, the nitrogen atoms closest to the methyl groups, form hydrogen bonds that are ∼0.1 Å longer than those from N2 and N4. A figure of these interactions, with distances, is provided in the Supporting Information. This asymmetry results in distinct differences between systems in which consecutive layers have a single chirality versus layers in which the chirality changes.

The partial enantiomeric resolution can be further understood in terms of the Ising model,

$$\hat{H} = \sum_i B_i s_i + \sum_{i,j} J_{ij} s_i s_j \qquad (1)$$

where each of the unit cell sites, *i*, is modeled by an effective "spin" s_i, (e.g., denoting $[(R)\text{-2-mpipH}_2]^{2+}$ and $[(S)\text{-2-mpipH}_2]^{2+}$ containing sites as $s_i = +1$ and $s_i = -1$, respectively), B_i denotes a site-specific bias energy, and J_{ij} denotes the interaction between spins at sites *i* and *j*. Based on the equal occurrence of $[(R)\text{-2-mpipH}_2]^{2+}$-predominant and $[(S)\text{-2-mpipH}_2]^{2+}$-predominant crystals, it is assumed that an initial seed nucleus is chosen randomly, with equal probabilities for $[(R)\text{-2-mpipH}_2]^{2+}$ and $[(S)\text{-2-mpipH}_2]^{2+}$ containing sites, so $B_i = 0$. Subsequent growth of the crystal then depends on this

dx.doi.org/10.1021/ic501736r | *Inorg. Chem.* 2014, 53, 12027−12035

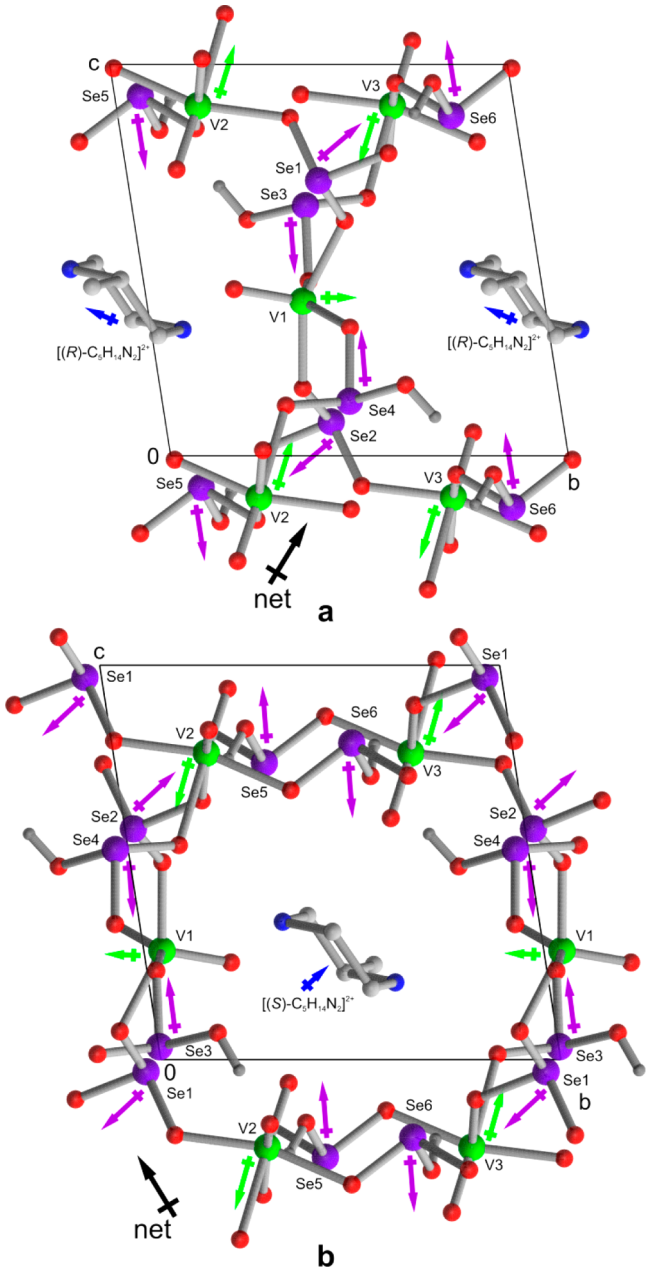

Figure 7. Ball-and-stick representations of **3a** and **3b**. Arrows indicate the approximate directions and magnitudes of the dipole moments for $[VO_6]$, $[VO_5]$, $[SeO_3]$, and $[C_5H_{14}N_2]^{2+}$ cations. The large black arrow represents the direction of the net dipole moment for **3a** and **3b**. Organic ammonium cation hydrogen atoms have been omitted for clarity.

seed nucleus. The proposed enantiomeric ordering *within* a two-dimensional layer, based upon interatomic distances and the structures of **3a** and **3b**, indicates that adjacent sites are strongly biased toward containing the same enantiomer, as discussed above. In the Ising model, this corresponds to a ferromagnetic ordering ($J_{ij} < 0$) with a large $|J_{ij}|$ for the intralayer interaction. The low crystallographic ordering *between* the layers indicates that adjacent layers have a preference for containing the same enantiomer, but that a significant fraction of sites contains a different enantiomer. The overall preference for preserving the same enantiomeric ordering (approximately 2:1) indicates that the interlayer coupling also corresponds to a ferromagnetic ($J_{ij} < 0$) Ising model, but with a smaller $|J_{ij}|$ allowing thermal fluctuations to give rise to disorder.

As perfect ordering within the *ab* plane is assumed, owing to strong intralayer interactions, the problem reduces to the one-dimensional Ising model,

$$\hat{H} = J \sum_i s_i s_{i+1} \tag{2}$$

where J is the interlayer coupling (assumed to occur only between nearest neighbors along the interlayer axis, and with uniform strength). The probability, p, of observing flipped (nonmajority) spins is

$$\ln \frac{p}{1-p} = \frac{-2J}{k_B T} \tag{3}$$

where k_B is the Boltzmann constant and T is the absolute temperature. The crystals were grown at T = 110 °C or k_BT = 33 meV. The mean probability of observing a "flipped" spin is p = 0.318, based upon the seven single crystal structures obtained for **1**, shown in Table 4. From this, the effective interaction energy is found to be J = 13 meV.

The 1D-Ising model allows us to better understand our results. First, unlike the 2D-Ising model, there are no phase transitions; this is consistent with the range in enantiomer ratios shown in Table 4. Second, the pair correlation function, $\langle s_i s_j \rangle$, of the 1D-Ising model decays exponentially with the distance between the sites $|i-j|$ at any finite temperature. This suggests that domain sizes should be small. Alternatively, if domain sizes were large, and the $[(R)\text{-2-mpipH}_2]^{2+}$ and $[(S)\text{-2-mpipH}_2]^{2+}$ *were* segregated into macroscopic domains within each crystal, crystallographic disorder would not be observed. These ordered structures would have Flack parameters deviating strongly from either 0 or 1, indicating an inversion twin. Thus, the small Flack parameters for **1a** and **1b**, shown in Table 3, are consistent with the small domain size predicted by the 1D-Ising model. Third, the 1D-Ising model allows us to put a bound on the possibility of modifying the overall enantiomeric preference by controlling the synthetic conditions. The hydrothermal synthesis of **1** can be performed between 90 and 125 °C, which in turn limits p to 0.30 and 0.32, respectively. Changing the temperature would have a relatively insignificant impact on the enantiomeric preference.

CONCLUSION

A direct correlation between the concentrations of the primary building units and product compositions is observed in the $VOSO_4/SeO_2$/2-methylpiperazine system. Adjustment of the initial reaction pH can be used to alter the ratio between $[HSeO_3]^-$ and $[SeO_3]^{2-}$, controlling the composition of the reaction product. In addition, partial resolution of $[(R)\text{-2-mpipH}_2]^{2+}$ and $[(S)\text{-2-mpipH}_2]^{2+}$ is caused by small differences in hydrogen-bonding interactions.

ASSOCIATED CONTENT

Supporting Information

Figures of the cation–anion interactions in **1**, **3a**, and **3b**, powder X-ray diffraction data and tables of bond valence sums for all compounds, and Hirshfeld-I partial atomic charges for **2**, **3a**, and **3b**. An X-ray crystallographic information file (CIF) for **1a**, **1b**, **2**, **3a**, and **3b**. This material is available free of charge via the Internet at http://pubs.acs.org.

dx.doi.org/10.1021/ic501736r | *Inorg. Chem.* 2014, 53, 12027–12035

AUTHOR INFORMATION

Corresponding Author

*Haverford College, 370 Lancaster Avenue, Haverford, PA 19041, United States. Tel: (610) 896 2949. Fax: (610) 896 4963. E-mail: anorquis@haverford.edu. http://www.haverford.edu/chem/Norquist/.

Notes

The authors declare no competing financial interest.

ACKNOWLEDGMENTS

The authors acknowledge support from the NSF (Award No. DMR-1307801), the Henry Dreyfus Teacher-Scholar Awards Program, and grants to Haverford College from the HHMI Undergraduate Science Education Program. M.Z. acknowledges support for the purchase of a diffractometer from the NSF Grant 0087210, the Ohio Board of Regents Grant CAP-491, and Youngstown State University. This research used computational resources of the National Energy Research Scientific Computing Center (NERSC), which is supported by the Office of Science of the U.S. Department of Energy under Contract No. DE-AC02-05CH11231.

REFERENCES

(1) Cheetham, A. K.; Ferey, G.; Loiseau, T. *Angew. Chem., Int. Ed.* **1999**, *38*, 3268−3292.
(2) Cundy, C. S.; Cox, P. A. *Chem. Rev.* **2003**, *103*, 663−701.
(3) Haushalter, R. C.; Mundi, L. A. *Chem. Mater.* **1992**, *4*, 31−48.
(4) Ferey, G. *J. Fluorine Chem.* **1995**, *72*, 187−193.
(5) Rao, C. N. R.; Natarajan, S.; Neeraj, S. *J. Am. Chem. Soc.* **2000**, *122*, 2810−2817.
(6) Rabenau, A. *Angew. Chem., Int. Ed. Engl.* **1985**, *24*, 1026−1040.
(7) Ferey, G. *Chem. Mater.* **2001**, *13*, 3084−3098.
(8) Rao, C. N. R.; Behera, J. N.; Dan, M. *Chem. Soc. Rev.* **2006**, *35*, 375−387.
(9) Glor, E. C.; Blau, S. M.; Yeon, J.; Zeller, M.; Shiv Halasyamani, P.; Schrier, J.; Norquist, A. J. *J. Solid State Chem.* **2011**, *184*, 1445−1450.
(10) Yu, J.; Xu, R. *Acc. Chem. Res.* **2010**, *43*, 1195−1204.
(11) Rao, C. N. R.; Natarajan, S.; Choudhury, A.; Neeraj, S.; Ayi, A. A. *Acc. Chem. Res.* **2001**, *34*, 80−87.
(12) Murugavel, R.; Walawalkar, M. G.; Dan, M.; Roesky, H. W.; Rao, C. N. R. *Acc. Chem. Res.* **2004**, *37*, 763−774.
(13) Rao, C. N. R.; Dan, M.; Behera, J. N. *Pure Appl. Chem.* **2005**, *77*, 1655−1674.
(14) Halasyamani, P.; Willis, M. J.; Stern, C. L.; Lundquist, P. M.; Wong, G. K.; Poeppelmeier, K. R. *Inorg. Chem.* **1996**, *35*, 1367−1371.
(15) Norquist, A. J.; Heier, K. R.; Stern, C. L.; Poeppelmeier, K. R. *Inorg. Chem.* **1998**, *37*, 6495−6501.
(16) Thomas, P. M.; Norquist, A. J.; Doran, M. B.; O'Hare, D. *J. Mater. Chem.* **2003**, *13*, 88−92.
(17) Veltman, T. R.; Stover, A. K.; Narducci Sarjeant, A.; Ok, K. M.; Halasyamani, P. S.; Norquist, A. J. *Inorg. Chem.* **2006**, *45*, 5529−5537.
(18) Nelson, J. H.; Johnston, A. R.; Narducci Sarjeant, A.; Norquist, A. J. *Solid State Sci.* **2007**, *9*, 472−484.
(19) Norquist, A. J.; Doran, M. B.; Thomas, P. M.; O'Hare, D. *Dalton Trans.* **2003**, 1168−1175.
(20) Stover, A. K.; Gutnick, J. R.; Narducci Sarjeant, A.; Norquist, A. J. *Inorg. Chem.* **2007**, *46*, 4389−4391.
(21) Hubbard, D. J.; Johnston, A. R.; Sanchez Casalongue, H.; Narducci Sarjeant, A.; Norquist, A. J. *Inorg. Chem.* **2008**, *47*, 8518−8525.
(22) Choyke, S. J.; Blau, S. M.; Larner, A. A.; Narducci Sarjeant, A.; Yeon, J.; Halasyamani, P. S.; Norquist, A. J. *Inorg. Chem.* **2009**, *48*, 11277−11282.
(23) Monnier, A.; Schuth, F.; Huo, Q.; Kumar, D.; Margolese, D.; Maxwell, R. S.; Stucky, G. D.; Krishnamurty, M.; Petroff, P.; Firouzi, A.; Janicke, M.; Chmelka, B. F. *Science* **1993**, *261*, 1299−1303.
(24) Huo, Q.; Margolese, D. I.; Ciesla, U.; Feng, P.; Gier, T. E.; Sieger, P.; Leon, R.; Petroff, P. M.; Schueth, F.; Stucky, G. D. *Nature* **1994**, *368*, 317−321.
(25) Tolbert, S. H.; Landry, C. C.; Stucky, G. D.; Chmelka, B. F.; Norby, P.; Hanson, J. C.; Monnier, A. *Chem. Mater.* **2001**, *13*, 2247−2256.
(26) El Haskouri, J.; Roca, M.; Cabrera, S.; Alamo, J.; Beltran-Porter, A.; Beltran-Porter, D.; Marcos, M. D.; Amoros, P. *Chem. Mater.* **1999**, *11*, 1446−1454.
(27) Casalongue, H. S.; Choyke, S. J.; Narducci Sarjeant, A.; Schrier, J.; Norquist, A. J. *J. Solid State Chem.* **2009**, *182*, 1297−1303.
(28) Chang, K. B.; Hubbard, D. J.; Zeller, M.; Schrier, J.; Norquist, A. J. *Inorg. Chem.* **2010**, *49*, 5167−5172.
(29) Koffer, J. H.; Olshansky, J. H.; Smith, M. D.; Hernandez, K. J.; Zeller, M.; Ferrence, G. M.; Schrier, J.; Norquist, A. J. *Cryst. Growth Des.* **2013**, *13*, 4504−4511.
(30) Olshansky, J. H.; Thao Tran, T.; Hernandez, K. J.; Zeller, M.; Halasyamani, P. S.; Schrier, J.; Norquist, A. J. *Inorg. Chem.* **2012**, *51*, 11040−11048.
(31) Smith, M. D.; Blau, S. M.; Chang, K. B.; Zeller, M.; Schrier, J.; Norquist, A. J. *Cryst. Growth Des.* **2011**, *11*, 4213−4219.
(32) Olshansky, J. H.; Blau, S. M.; Zeller, M.; Schrier, J.; Norquist, A. J. *Cryst. Growth Des.* **2011**, *11*, 3065−3071.
(33) Gutnick, J. R.; Muller, E. A.; Narducci Sarjeant, A.; Norquist, A. J. *Inorg. Chem.* **2004**, *43*, 6528−6530.
(34) Muller, E. A.; Cannon, R. J.; Narducci Sarjeant, A.; Ok, K. M.; Halasyamani, P. S.; Norquist, A. J. *Cryst. Growth Des.* **2005**, *5*, 1913−1917.
(35) Bruker AXS Inc.: Madison, WI, USA, 2009.
(36) Altomare, A.; Cascarano, G.; Giacovazzo, C.; Guagliardi, A. *J. Appl. Crystallogr.* **1993**, *26*, 343−350.
(37) Betteridge, P. W.; Carruthers, J. R.; Cooper, R. I.; Prout, K.; Watkin, D. J. *J. Appl. Crystallogr.* **2003**, *36*, 1487.
(38) Dowty, E. Shape Software: Kingsport, TN, USA, 2002.
(39) Brown, I. D.; Altermatt, D. *Acta Crystallogr., Sect. B* **1985**, *41*, 244−247.
(40) Brese, N. E.; O'Keeffe, M. *Acta Crystallogr., Sect. B* **1991**, *47*, 192−197.
(41) Gonze, X.; Beuken, J. M.; Caracas, R.; Detraux, F.; Fuchs, M.; Rignanese, G. M.; Sindic, L.; Verstraete, M.; Zerah, G.; Jollet, F.; Torrent, M.; Roy, A.; Mikami, M.; Ghosez, P.; Raty, J. Y.; Allan, D. C. *Comput. Mater. Sci.* **2002**, *25*, 478−492.
(42) Gonze, X.; Amadon, B.; Anglade, P. M.; Beuken, J. M.; Bottin, F.; Boulanger, P.; Bruneval, F.; Caliste, D.; Caracas, R.; Cote, M.; Deutsch, T.; Genovese, L.; Ghosez, P.; Giantomassi, M.; Goedecker, S.; Hamann, D. R.; Hermet, P.; Jollet, F.; Jomard, G.; Leroux, S.; Mancini, M.; Mazevet, S.; Oliveira, M. J. T.; Onida, G.; Pouillon, Y.; Rangel, T.; Rignanese, G. M.; Sangalli, D.; Shaltaf, R.; Torrent, M.; Verstraete, M. J.; Zerah, G.; Zwanziger, J. W. *Comput. Phys. Commun.* **2009**, *180*, 2582−2615.
(43) Momma, K.; Izumi, F. *J. Appl. Crystallogr.* **2008**, *41*, 653−658.
(44) Bultinck, P.; Van Alsenoy, C.; Ayers, P. W.; Carbo-Dorca, R. *J. Chem. Phys.* **2007**, *126*, 144111.
(45) Bultinck, P.; Ayers, P. W.; Fias, S.; Tiels, K.; Van Alsenoy, C. *Chem. Phys. Lett.* **2007**, *444*, 205−208.
(46) Gaigalas, G.; Froese Fischer, C. *Comput. Phys. Commun.* **1996**, *98*, 255−264.
(47) Smith, M. D.; Blau, S. M.; Chang, K. B.; Tran, T. T.; Zeller, M.; Halasyamani, P. S.; Schrier, J.; Norquist, A. J. *J. Solid State Chem.* **2012**, *195*, 86−93.
(48) Chang, K. B.; Smith, M. D.; Blau, S. M.; Glor, E. C.; Zeller, M.; Schrier, J.; Norquist, A. J. *Cryst. Growth Des.* **2013**, *13*, 2190−2197.
(49) Engelen, B.; Boldt, K.; Unterderweide, K.; Baeumer, U. *Z. Anorg. Allg. Chem.* **1995**, *621*, 331−339.
(50) Micka, Z.; Nemec, I.; Vojtisek, P.; Ondracek, J. *J. Solid State Chem.* **1996**, *122*, 338−342.
(51) Dai, Z.; Li, G.; Shi, Z.; Fu, W.; Dong, W.; Xu, J.; Feng, S. *Solid State Sci.* **2004**, *6*, 91−96.

(52) Norquist, A. J.; Doran, M. B.; O'Hare, D. *Inorg. Chem.* **2005**, *44*, 3837−3843.
(53) Tudo, J.; Jolibois, B.; Laplace, G.; Nowogrocki, G.; Abraham, F. *Acta Crystallogr., Sect. B* **1979**, *B35*, 1580−1583.
(54) Chang, F. M.; Jansen, M.; Schmitz, D. *Acta Crystallogr., Sect. C: Cryst. Struct. Commun.* **1983**, *C39*, 1497−1498.
(55) Morris, R. E.; Harrison, W. T. A.; Stucky, G. D.; Cheetham, A. K. *J. Solid State Chem.* **1991**, *94*, 227−235.
(56) Van Damme, S.; Bultinck, P.; Fias, S. *J. Chem. Theory Comput.* **2009**, *5*, 334−340.
(57) Kim, J.-H.; Baek, J.; Halasyamani, P. S. *Chem. Mater.* **2007**, *19*, 5637−5641.
(58) Maggard, P. A.; Nault, T. S.; Stern, C. L.; Poeppelmeier, K. R. *J. Solid State Chem.* **2003**, *175*, 27−33.
(59) Izumi, H. K.; Kirsch, J. E.; Stern, C. L.; Poeppelmeier, K. R. *Inorg. Chem.* **2005**, *44*, 884−895.
(60) Fabian, L.; Brock, C. P. *Acta Crystallogr., Sect. B: Struct. Sci.* **2010**, *B66*, 94−103.

dx.doi.org/10.1021/ic501736r | *Inorg. Chem.* 2014, 53, 12027−12035